Title: Analysis of caspase-mediated regulation of the cGAS/STING pathway in Kaposi's sarcoma-associated herpesvirus lytic infection reveals a dramatic cellular heterogeneity in type I interferon responses

Authors: Tate Tabtieng[1,2,4], Rachel C. Lent[1,3], Alvaro Monago Sanchez[1,5], Marta Maria Gaglia[1,2,3]

[1] Department of Molecular Biology and Microbiology, Tufts University School of Medicine, Boston, MA

[2] Program in Biochemistry, Tufts University Graduate School of Biomedical Sciences, Boston, MA

[3] Program in Molecular Microbiology, Tufts University Graduate School of Biomedical Sciences, Boston, MA

[4] Present address: Generate Biomedicines, Cambridge, MA

[5] Present address: Master in Molecular Biomedicine Program, Graduate School, Universidad Autonoma de Madrid

Correspondence to: Marta Maria Gaglia, Marta.Gaglia@tufts.edu

Summary

During the ongoing virus-host arms race, viruses have evolved numerous immune subversion strategies aimed at the production of type I interferons (IFNs)[1]. This focus on IFN evasion highlights the essentiality of these cytokines in controlling viral infections. Apoptotic caspases have recently emerged as important regulators of type I IFN signaling in both non-infectious contexts and during viral infection[2–5]. Surprisingly, they promote viral immune evasion despite being widely considered anti-viral from triggering cell death[2–5]. Indeed, we previously discovered that the AIDS-associated oncogenic gammaherpesvirus Kaposi's sarcoma-associated herpesvirus (KSHV) exploits caspase-8 activity to suppress the antiviral type I IFN response and promote viral replication[5]. However, the mechanisms of this novel viral immune evasion strategy are poorly understood, particularly how caspase-8 antagonizes IFN signaling. Here we show that caspase activity inhibits the DNA sensor cGAS[6] during KSHV lytic replication to block IFN induction. Furthermore, we use single-cell RNA-sequencing to reveal that the potent antiviral state conferred upon caspase inhibition is mediated by an exceptionally small percentage of infected cells expressing IFN-β, thus uncovering further complexity of IFN regulation during viral infection. Collectively, these results provide insight into multiple levels of type I IFN regulation by the cell and the way in which viruses co-opt them for immune evasion. Unraveling these mechanisms can inform targeted therapeutic strategies for viral infections and reveal cellular mechanisms of regulating interferon signaling in the context of cancer and chronic inflammatory diseases.

Upon infection of a host cell, viral nucleic acids are sensed by host cell pattern recognition receptors such as the cytosolic DNA sensor cGAS and RNA sensor RIG-I[7]. These sensors signal through adaptor proteins (STING and MAVS, respectively) and the kinases TBK1 and IKKε to activate the transcription factor IRF3 and trigger induction of type I IFN cytokines[7]. Type I IFNs in turn signal to both the producing and neighboring cells to express interferon stimulated genes (ISGs) that limit viral replication and infection[8]. As this is a strong antiviral response, all viruses have evolved one or more strategies to block IFN induction[1]. Indeed, KSHV induces minimal type I IFN responses when reactivating from latency[5,9], demonstrating it can strongly block this response. While many viral encoded factors directly target the type I IFN response, viruses have also evolved strategies to usurp cellular pathways to counteract immune responses. While apoptotic caspases are canonically thought to be antiviral by facilitating cell death of infected cells, recent studies have demonstrated caspase-dependent inhibition of innate immune signaling during apoptosis and viral infection[2–5]. Caspase-3 and -7 can directly cleave cGAS, MAVS, and IRF3 to block type I IFN signaling[4]. In addition, we established that KSHV exploits caspase-8 activity to suppress the type I IFN response[5]. While normally KSHV reactivation does not induce a strong type I IFN response, lytically infected cells express and secrete high levels of IFN-β , if caspase-8 is inhibited[5]. KSHV uses this mechanism to promote viral replication while at the same time preventing caspase-mediated cell death[5]. However, it is unclear how caspase-8 enacts this previously undescribed IFN regulatory function.

We previously showed that the type I IFN response that occurs upon caspase inhibition is dependent on TBK1[5], a kinase that can be activated by several pathogen sensors[7]. To discern which pathway mediates IFN induction and is inhibited by caspase activity during KSHV infection, we knocked down the key adaptor proteins for DNA sensing, STING, and RNA

sensing, MAVS (Supp Fig. 1, Fig. 1). For these experiments, we used iSLK.219 cells, which are latently infected with recombinant rKSHV.219 that expresses GFP constitutively and RFP under the control of a KSHV lytic promoter[10]. These cells also express an exogenous copy of the KSHV master lytic regulator RTA under a doxycycline inducible promoter, so that reactivation of the viral lytic replication cycle can be induced by doxycycline treatment[10] . Knockdown of STING and MAVS effectively and specifically attenuated IFN-β induction through their respective signaling pathways after stimulation with plasmid DNA or poly(I:C) (Supp. Fig. 1B, D). Importantly, IFN-β induction upon caspase inhibition was severely reduced with STING depletion, suggesting that caspase activity targets STING-dependent type I IFN signaling during KSHV replication (Fig. 1A). Moreover, upon STING knock-down, caspase inhibitors no longer caused a reduction in KSHV replication, which we previously showed is a result of type I IFN induction[5] (Fig.1B). MAVS knockdown also partially reduced IFN-β expression upon caspase inhibition (Fig.1A), but it also substantially decreased the expression of the viral mRNA ORF37 even in the absence of caspase inhibitors (Fig.1B), suggesting that the reduced IFN-β induction in this case may be due to lower levels of KSHV reactivation in the absence of MAVS.

To confirm that caspase activity predominantly targets IFN-β induction through the DNA sensing pathway, we tested two DNA sensors that act upstream of STING and were previously reported to sense KSHV, cGAS[9,11,12] and the nuclear localized sensor IFI16[13]. Knockdown of cGAS, but not IFI16, reduced IFN-β induction upon caspase inhibition (Fig.1C). As expected from the effects on IFN-β induction and similar to STING knockdown, cGAS knockdown also prevented the inhibition in ORF37 expression mediated by caspase inhibition (Fig.1D), suggesting it blocked IFN-β secretion and the consequent reduction in viral replication. In

contrast, IFI16 knockdown did not hinder this pro-viral caspase function (Fig.1C-D). Consistent with the effects of cGAS knockdown, we also found that pharmacological inhibition of cGAS with RU.521 reduced IFN-β (Fig. 1F) and ISG15 (Supp. Fig. 2A) induction upon caspase inhibition. These findings suggest that caspase activity targets the cGAS-STING DNA sensing pathway during KSHV lytic replication.

To corroborate these results, we also tested whether there was differential activation of the cGAS/STING pathway in the presence vs. absence of caspase activity. After binding DNA, cGAS synthesizes the cyclic dinucleotide 2'3'-cGAMP, which in turn binds and activates STING[14]. 2'3'-cGAMP levels were increased upon caspase inhibition and were reduced by treatment with a cGAS inhibitor (Fig.1G). We also observed increased phosphorylation of the downstream proteins STING, TBK1, and IRF3, which indicates that they are activated upon caspase inhibition (Fig.1H). Taken together with our results from the knockdown experiments, these findings identify the target of caspases as a component or regulator of the cGAS/STING pathway that acts to promote activation or activity of cGAS.

We considered the possibility that the target was cGAS itself, as one report suggests that caspase-3 and -7 can cut cGAS during apoptosis and other viral infections[4]. However, we do not detect an overall reduction in cGAS levels or cGAS cleavage fragments during lytic reactivation (Fig. 1E). It is thus possible that caspases inhibit cGAS activity by targeting a key regulatory factor that modulates cGAS activity.

To determine if caspases also suppress the cGAS/STING pathway in a cell type that is physiologically relevant for KSHV infection and tumorigenesis, we examined the activity of caspases in BC3 cells, a KSHV-infected B cell line derived from a primary effusion lymphoma

(PEL) patient. Caspase-8 was also activated upon lytic reactivation of BC3 cells (Fig. 2A). Moreover, caspase inhibition increased expression of both IFN-β and several ISGs (Fig. 2B-D), and increased IRF3 phosphorylation (Fig. 2F). Consistent with what we observed in iSLK.219 cells, caspase inhibition potentiated 2'3'-cGAMP production in lytically reactivated BC3 cells (Fig. 2E). Moreover, inhibition of cGAS with RU.521 reduced the induction of IFN-β (Fig. 2G) and, to some extent, ISG15 (Supp Fig.2B), as well as IRF3 phosphorylation (Fig. 2F). These results strengthen our conclusion that caspases have a major role in inhibiting cGAS activity or activation to block IFN induction during KSHV lytic infection.

Since we know that not all iSLK.219 cells in the population re-enter the lytic cycle upon doxycycline addition, we carried out single-cell RNA sequencing (scRNAseq) on latently infected and uninfected cells, lytically infected and lytically infected cells treated with IDN-6556 to understand the cell-to-cell variability in reactivation and IFN signaling (Fig. 3A). We also included cells treated with IDN-6556 and anti-IFN antibodies to block paracrine signals (Fig. 3A, Supp. Fig. 3A). Analysis using the Seurat package[15,16] unbiasedly identified 13 clusters with different gene expression across the 4 samples (Fig. 3B). Analysis of the mapped reads showed that, as expected, there was a higher percentage of KSHV reads in cells that were lytically reactivated (Fig. 3C,D). Certain clusters were clearly enriched in KSHV transcripts (Fig.3C,E; Supp. Fig. 3E,F) and these corresponded to clusters that only appeared in the lytic samples (Fig. 3B,C). We further analyzed the type of genes that were seen in the different clusters in the lytic+vehicle sample, and saw that cells in only one cluster, cluster 12, appeared to have more than 25% KSHV reads and a substantial signal for late genes (Fig. 3E-G). Because our scRNAseq is directed at the 3' end of RNAs and many mRNAs in KSHV have the same 3' end[17,18], we were not able to conclusively discern expression of all the genes. However, analysis

of individual genes, as well as the KSHV.219 encoded GFP, RFP and puromycin (PAC) reporters agrees with the general picture obtained from percentage reads, with most clusters showing some lytic gene expression and only a few substantial lytic cycle reactivation (Fig. 3E). Moreover, we note that some of the clusters that expressed lytic genes did not express high levels of RFP (cluster 0, for example, Fig. 3E). Furthermore, analysis of the cell cycle status of the cells indicated that most of the cells were in G1, including cells in clusters with high levels of lytic genes, but that some of the clusters were enriched in cells in S or G2/M phase (Supp. Fig. 3G). Because KSHV lytic genes are expressed in several waves, termed early lytic, delayed early and late[19–21], we roughly categorized the clusters based on the pattern of lytic gene expression, as well as the cell cycle stage and the expression of IFNs. We classified clusters as "uninfected", "latent", "latent (diving)", "lytic (early)", "lytic (intermediate)", "lytic (late)", "lytic (early) and IFN+" (Fig. 3E, 3H). Figure 3H shows how the different clusters expanded and contracted in each sample. Addition of the caspase inhibitors reduced the percentage of cells in lytic clusters, an effect that was largely rescued by inhibition of paracrine IFN signaling with anti-IFN antibodies (Fig. 3H). Overall, these data confirm the wide variability in stage of reactivation of iSLK.219 cells and reveal that the RFP signal in iSLK.219 cells may underestimate the cells that are expressing lytic genes. Moreover, they recapitulate our bulk level findings on KSHV replication upon caspase inhibition.

An outstanding question from our bulk analysis was the source of the IFN-β in the caspase inhibitor treated samples, although we hypothesized that the lytically infected cells were producing it. Surprisingly, we found that only 3.8% of the cells in the caspase inhibitor treated samples expressed type I IFNs, particularly IFN-β, and that these were concentrated in clusters 9 and 11, which only appeared in the +IDN-6556 samples (Fig. 4B). None of the cells expressed

IFN-αs. Nonetheless, the IFN-β coming from these cells was sufficient to elicit a strong response in the entire population of cells, as indicated by the expression of interferon stimulated genes (ISGs) (Fig. 4C). Moreover, as we previously showed in bulk analysis, the type I IFN signaling reduced viral replication and gene expression across the population (Fig.3C, 4D-E). We examined the possibility that only a subset of cells makes IFN-β due to differential expression of viral genes. For example, IFN-β+ cells could lack expression of KSHV-encoded anti-IFN factors. In general, IFN-β+ cells expressed only early lytic genes and low levels of the RFP lytic marker (Fig. 4D-E). However, their expression pattern is similar to other clusters (Fig. 4D-E), such as cluster 0, that do not express IFN-β, suggesting differential expression of viral genes may not explain the restricted IFN-β expression pattern. Another possibility is that these cells express higher basal levels of genes in the type I IFN induction pathway and are thus more sensitive to IFN-inducing cues. This model was proposed in the case of other viral infections by Zhao *et al.*[22]. Analyzing these genes is complicated by the fact that many of them are themselves ISGs, as evidenced by the change in expression upon anti-IFN antibody treatment (Fig. 4F-G). Nonetheless, there was a clear enrichment of genes involved in the NF-κB signaling pathway (NFKB1, NFKB2, RELA, RELB) in the IFN-β+ clusters 9 and 11 (Fig. 4F-G). The NF-κB transcription factor is also needed for IFN-β transcription downstream of pathogen sensors, together with IRF3[7]. In addition, the gene whose expression best correlated with IFN-β+ was RHEBL1, a little-studied regulator of the NF-κB signaling pathway[23]. We also found increased phosphorylation of NF-κB and increased NF-κB levels in lytic cells treated with IDN-6556, showing that caspase activity also modulates NF-κB activation (Fig. 4H). It is thus possible that high NF-κB expression is needed to induce IFN in these cells. To ensure that the variability in IFN-β induction is not an artifact of a limit of detection by scRNAseq we constructed a cell line

that expresses the TagBFP protein under the control of the IFN-β promoter. When the lytic cycle was induced in these cells concomitantly with caspase inhibitor treatment, we found that ~1% of the cells became TagBFP+ (Fig. 4I). The percentage was similar among RFP positive and negative cells, which is consistent with our scRNAseq results. Overall, these data show that only a few cells induce IFNs even under caspase inhibition.

Collectively, this study reveals novel mechanistic insight into multiple levels of type I IFN regulation during KSHV infection. The cGAS/STING pathway has emerged in recent years as a crucial component of the innate immune response to DNA viruses and various other pathogens[6]. This is highlighted by the multitude of strategies employed by pathogens[24], including herpesviruses[25], to disrupt the cGAS/STING pathway at multiple levels. While this immunosuppression is often driven by viral encoded proteins, we have uncovered an intriguing mechanism in KSHV infection, which involves the hijacking of a host cell component, caspase-8, to subvert immune activation and viral clearance. While caspase-3 has been described to directly target cGAS in an apoptotic setting and some viral infections[4], caspase-8 activity predominantly mediates the type I IFN suppression observed in KSHV infected cells without triggering apoptosis, and caspase-3 activity is dispensable[5]. These observations in conjunction with the current study suggest an unexpected type I IFN regulatory function of non-apoptotic caspase-8 activity mediated by targeting the cGAS/STING pathway. Caspase-8 is an attractive therapeutic target that could be exploited to potentiate cGAS/STING-mediated immune responses for viral clearance. This could have far reaching implications for other pathologies, as regulation of the cGAS/STING pathway is fundamental in various inflammatory diseases and in tumor immunity[26,27], and thus is a current focus of intensive drug discovery research efforts.

The notable cellular heterogeneity in type I IFN production reveals an additional layer of complexity and regulation of innate immune responses during KSHV infection. We detect an exceptionally small fraction of IFN-β+ cells upon caspase inhibitor treatment (< 5%, Fig. 4B). Remarkably, this small IFN-β+ cell population still induces a robust IFN response in the population (Fig. 4C). On a practical level, the high heterogeneity in IFN-β expression complicates our analysis of caspase-8 regulation of cGAS. It is possible that the upstream portions of the pathway (i.e. cGAS) are also only active in the IFN-β+ cells, and that cell sorting may be needed to detect differences in the levels of the direct target(s) of caspase-8 in IFN regulation. Alternatively, it is possible that only a subset of the cells in which the IFN induction pathway is activated end up expressing IFN-β. In support of this idea, we were able to easily detect phosphorylation of many of the components of the IFN induction pathway using bulk analysis (Figs. 1H, 2F, 4H).

Other studies have also showed a small number of cells that respond to infection in a population in a number of other viruses[22,28–33]. Interestingly, several of these studies investigated infections in immune cell types and fibroblasts and saw higher percentages of responding cells (10-30%)[22,28,29]. In contrast, iSLK.219 cells are of epithelial origin[34]. Epithelial cells are often the first exposed to invading pathogens and mount responses that alert and prime surrounding cells to counteract viral spread. Therefore, it is possible that epithelial cell responsiveness is even more tightly regulated to prevent inadvertent activation of the pathway. Consistent with this idea, influenza A virus and SARS coronavirus 2 infection of epithelial cells also elicit responses in a small minority of cells[30–32].

It is unclear what the source of the heterogeneity is in KSHV-infected cells. Viral gene expression, and in particular in viral immune regulators, is often considered the reason for limited type I IFN responses[32]. However, we find that IFN-β+ have a similar expression pattern as cells that do not make IFNs (Fig. 4D,E). While we cannot exclude the possibility that one specific gene is responsible for the difference, especially since we do not reliably detect all viral genes, these results suggest that inherent differences in the cells govern the heterogeneity. Stochasticity in gene expression, which is common among cytokines, has also been proposed as driver of type I IFN expression heterogeneity. Zhao *et al.* suggested some of this stochasticity may be epigenetically encoded[22], reducing the number of cells that are able to express type I IFN, perhaps to prevent over-activation and inflammation. Paracrine IFN signaling is also thought to influence and modulate heterogeneity[33]. This cell-cell communication may fine tune immune signal amplification in a cell density-dependent manner. Indeed, we observe 3.8% IFN-β+ cells in the IDN-6556 treated sample, but only 1.6% IFN-β+ cells in the sample treated with IDN-6556 and anti-IFN antibodies that block paracrine IFN signaling. This reinforces the notion of self-amplification of the type I IFN response as a layer of regulation that directs selective robust responses in appropriate contexts for infection control, while avoiding tissue damage from unnecessary inflammation.

Methods

Cell lines, reagents, and treatments

All cells were cultured at 37 °C and 5% CO_2 conditions. iSLK.219, iSLK.219-IFNBp-BFP, iSLK.RTA[10], and HEK293T cells were grown in Dulbecco's modified Eagle's medium (DMEM; Life Technologies) supplemented with 10% fetal bovine serum (FBS) (HyClone). BC3 cells were grown in RPMI supplemented with 20% FBS, 2 mM GlutaMAX supplement, and 55 μM β-mercaptoethanol (Gibco/Thermo Fisher). iSLK.219 cells were reactivated with 1 μg/ml of doxycycline (Thermo Fisher). Reactivation was confirmed visually for all iSLK.219 samples by examining the appearance of RFP-positive cells (RFP is driven by the lytic PAN promoter). BC3 cells were reactivated with 20 ng/ml of TPA for 48 h. iSLK.219-IFNBp-BFP cells were generated by transducing iSLK.219 cells with lentiviruses containing pJP1_IFNBp-tagBFP. This construct is based on pLJM1-GFP, a gift from David Sabatini (Addgene plasmid # 19319 ; http://n2t.net/addgene:19319 ; RRID:Addgene_19319)[35]. The CMV promoter in this plasmid was replaced with a human IFN-β promoter subcloned from a luciferase reporter construct (kind gift of Michaela Gack) and the GFP sequence was replaced with a TagBFP sequence. In addition, the antibiotic resistance gene was changed from a puromycin resistance to a zeocin resistance gene. Lentiviral packaging was carried out using packaging plasmids pMDLg/pRRE (Addgene plasmid # 12251 ; http://n2t.net/addgene:12251 ; RRID:Addgene_12251), Addgene plasmid # 12253 ; http://n2t.net/addgene:12253 ; RRID:Addgene_12253) and pMD2.G (Addgene plasmid # 12259 ; http://n2t.net/addgene:12259 ; RRID:Addgene_12259), kind gifts from Didier Trono[36]. Where indicated, cells were treated with vehicle (dimethyl sulfoxide [DMSO]; Sigma-Aldrich), 10 μM IDN-6556 (MedChem Express or Selleck Chemicals), 24.1 μM RU.521 (Invivogen), 1:50, 1:100, or 1:500 dilutions of a mixture of neutralizing antibodies against type I IFNs (PBL Assay Science). The concentrations of all drug treatments were chosen

based on common concentrations used in previously published studies. For DNA treatment, cells were transfected with 400 ng/well of plasmid DNA (pcDNA 3.1+) complexed with 0.8 µl/well of FuGENE (Promega) in Opti-MEM I (Life Technologies) in a 24-well plate for 3 h prior to sample collection. For poly(I·C) treatment, cells were transfected with 5 µg/ml poly(I·C) precomplexed with LyoVec transfection reagent (Invivogen) in Opti-MEM I (Life Technologies) for 3 h prior to sample collection.

siRNA knockdown

iSLK.219 cells were transfected while in suspension (reverse transfection) with 10 nM siRNAs against STING (HSS139156), MAVS (HSS148537), cGAS (siRNA#1, HSS132955; siRNA#2, HSS132956), IFI16 (siRNA#1, HSS105205; siRNA#2, HSS105206), or a nontargeting siRNA (12935300) at a density of 16,700 cells/cm^2, using the Lipofectamine RNAiMAX transfection reagent (Life Technologies/Thermo Fisher) per the manufacturer's protocol. Six hours later, the medium was replaced. The lytic cycle was induced two days later. For cGAS knockdowns, the reverse transfection process was done twice, once 2 days prior to induction and a second time on the day of lytic cycle induction. All siRNAs were obtained from Life Technologies/Thermo Fisher.

Realtime quantitative polymerase chain reaction (RT-qPCR)

For RNA analysis, iSLK.219 cells were seeded at a density of 33,000 cells per well in a 24-well plate, and the lytic cycle was induced by the addition of doxycycline (1 µg/ml). RNA

samples were collected at the indicated time points in RNA lysis buffer (Zymo Research). BC3 cells were seeded at 500,000 cells per ml and induced using TPA for 48 h. One ml of the cells was collected, and the cell pellet was lysed in RNA lysis buffer (Zymo Research). Total RNA was extracted using the Quick-RNA MiniPrep kit (Zymo Research) by following the manufacturer's protocol. For human and mouse mRNA measurements, cDNA was prepared using an iScript cDNA synthesis kit (Bio-Rad) per the manufacturer's protocol. For viral mRNA measurements, cDNA was prepared using AMV RT (Promega) per the manufacturer's protocol, using a cocktail of primers targeted at KSHV genes and 18S rRNA in order to obtain strand-specific measurements. In all cases, 18S rRNA levels were used as an internal standard to calculate relative mRNA levels. Real-time quantitative PCR (RT-qPCR) was performed using iTaq Universal SYBR green supermix (Bio-Rad) in a CFX Connect real-time PCR detection system (Bio-Rad). No-template and no-RT controls were included in each replicate. CFX Manager software was used to analyze the data. Primers are listed in Table.

Protein analysis

iSLK.219 cells were seeded at a density of 167,000 cells per well in a 6-well plate and treated with doxycycline (1 μg/ml). Lysates were collected at the indicated time points. Cells were lysed in radioimmunoprecipitation assay (RIPA) buffer (50 mM Tris-HCl, pH 7.4, 150 mM NaCl, 2 mM EDTA, 0.5% sodium deoxycholate, 0.1% SDS, 1% NP-40) or an NP-40-only buffer for caspase blots and phospho-protein blots (50 mM Tris-HCl, pH 7.4, 150 mM NaCl, 1 mM EDTA, 0.5% NP-40) supplemented with 50 μg/ml phenylmethylsulfonyl fluoride (PMSF; G-

Biosciences) and cOmplete protease cocktail inhibitor (Roche). Samples were separated by SDS-PAGE and transferred to polyvinylidene difluoride (PVDF) membranes. The following Cell Signaling Technologies antibodies were used on PVDF membranes blocked in 5% milk in Tris-buffered saline with 0.1% Tween 20 (TBST) at 1:1,000 dilution in 5% milk in TBST: anti-cGAS (D1D3G) (no. 15102). The following Cell Signaling Technologies antibodies were used with PVDF membranes blocked in 5% bovine serum albumin (BSA; Thermo Fisher) in TBST at 1:1,000 dilution in 5% BSA in TBST: anti-caspase-8 (no. 9746), anti-cleaved caspase-8 (no. 9496), anti-IRF3 (D83B9) (no. 4302), anti-phospho-IRF3 Ser396 (4D4G) (no. 4947), anti-TBK1 (D1B4) (no. 3504), anti-phospho-TBK1 Ser172 (D52C2) (no. 5483), anti-STING (D2P2F) (no. 13647), anti-phospho-STING Ser366 (D7C3S) (no. 19781), and anti-β-tubulin (9F3) (no. 2128). Anti-IFI16 (ab169788; 1:1000, Abcam) and anti-β-actin (ab8229; 1:500, Abcam) was diluted in 5% BSA in TBST and used with PVDF membranes blocked in 5% BSA in TBST. Anti-MAVS (sc-166583, 1:1000 dilution; Santa Cruz Biotechnology) was diluted in 0.5% milk in phosphate-buffered saline with 0.1% Tween 20 (PBST) and used with PVDF membranes blocked in 5% milk in PBST. Horseradish peroxidase (HRP)-conjugated goat anti-rabbit IgG and goat anti-mouse IgG (both 1:5,000 in blocking buffer) were purchased from Southern Biotechnology. HRP-conjugated donkey anti-goat IgG (1:5,000 in 0.5% milk in PBST) was purchased from Santa Cruz Biotechnology. All membranes were exposed using Pierce ECL Western blotting substrate (Thermo Fisher) and imaged with a Syngene G:Box Chemi XT4 gel doc system.

cGAMP ELISA

Cell lysates were harvested 4 days post reactivation in RIPA and subjected to enzyme-linked immunosorbent assay (ELISA) analysis for 2’3’-cGAMP (Cayman Chemical) according to the manufacturers' protocols. Each biological replicate consisted of three technical replicates per condition.

Single cell RNA sequencing

iSLK.219 and iSLK.RTA cells were seeded onto T25 flasks at a density of 16,700 cells/cm^2 and induced with doxycycline in the presence or absence of IDN-6556 (10 μM) and a mixture of neutralizing antibodies against type I IFNs at a 1:500 dilution (39000-1; PBL Assay Science). The media was replaced at day 2 post reactivation with fresh doxycycline, IDN-6556, and type I IFN neutralizing antibodies. Cells were harvested at day 4 post reactivation, washed twice with PBS, and strained to create single cell suspensions at a concentration of 1,000,000/ml. For individual cell analysis, we used the 10x Genomics platform. Gel Bead-in-Emulsion (GEM) generation was done according to the manufacturer’s protocol (10X genomics, version 3). Single cell cDNA libraries were generated according to manufacturer’s protocol. Paired-end sequencing with 75 cycle read length was performed on an Illumina Nextseq at Tufts Genomics Facility. Raw sequencing data were processed using the 10X Genomics CellRanger (3.0.0) software. Reads were aligned to a reference genome containing the human genome (GRCh38), the KSHV genome (GQ994935.1) and the additional sequence of the RFP-GFP insertion cassette. This third reference was added because the GQ994935.1 reference genome corresponds to the KSHV BAC16 genome, whereas our cells contain the rKSHV.219 virus. A full reference for

rKSHV.219 is not available. We thus amplified the missing region and sequenced it using Sanger sequencing. Integration and clustering analyses were done in R version 3.6.1 using the Seurat package (version 3.1.1.9021)[15,16]. Cell cycle analysis was done according Tirosh *et al.*[37].

Statistical analysis

All statistical analysis was performed using GraphPad Prism version 8.4.2 or later (GraphPad Software, La Jolla California USA, www.graphpad.com). Statistical significance was determined by Student's *t*-test or analysis of variance (ANOVA) followed by a *post hoc* multiple comparison test (Dunnett's, Sidak's or Tukey's) when multiple comparisons were required. All data are plotted as mean ± standard deviation.

Acknowledgements

We thank members of the Gaglia laboratory for suggestion and feedback. This work was supported by American Cancer Society grant 131320-RSG-17-189-01-MPC to MMG. TT was supported by the Tufts Collaborative Cancer Biology Award. RCL is supported by NIH training grant T32 GM007310.

References

1. García-Sastre, A. Ten Strategies of Interferon Evasion by Viruses. *Cell Host & Microbe* **22**, 176–184 (2017).
2. White, M. J. *et al.* Apoptotic caspases suppress mtDNA-induced STING-mediated type I IFN production. *Cell* **159**, 1549–1562 (2014).

3. Rongvaux, A. *et al.* Apoptotic caspases prevent the induction of type I interferons by mitochondrial DNA. *Cell* **159**, 1563–1577 (2014).
4. Ning, X. *et al.* Apoptotic Caspases Suppress Type I Interferon Production via the Cleavage of cGAS, MAVS, and IRF3. *Molecular Cell* **74**, 19-31.e7 (2019).
5. Tabtieng, T., Degterev, A. & Gaglia, M. M. Caspase-Dependent Suppression of Type I Interferon Signaling Promotes Kaposi's Sarcoma-Associated Herpesvirus Lytic Replication. *Journal of Virology* **92**, e00078-18 (2018).
6. Cai, X., Chiu, Y.-H. & Chen, Z. J. The cGAS-cGAMP-STING Pathway of Cytosolic DNA Sensing and Signaling. *Molecular Cell* **54**, 289–296 (2014).
7. Wu, J. & Chen, Z. J. Innate immune sensing and signaling of cytosolic nucleic acids. *Annu. Rev. Immunol.* **32**, 461–488 (2014).
8. Schoggins, J. W. Interferon-stimulated genes: roles in viral pathogenesis. *Curr Opin Virol* **6**, 40–46 (2014).
9. Zhang, G. *et al.* Cytoplasmic isoforms of Kaposi sarcoma herpesvirus LANA recruit and antagonize the innate immune DNA sensor cGAS. *PNAS* **113**, E1034–E1043 (2016).
10. Myoung, J. & Ganem, D. Generation of a doxycycline-inducible KSHV producer cell line of endothelial origin: maintenance of tight latency with efficient reactivation upon induction. *J. Virol. Methods* **174**, 12–21 (2011).
11. Ma, Z. *et al.* Modulation of the cGAS-STING DNA sensing pathway by gammaherpesviruses. *Proc. Natl. Acad. Sci. U.S.A.* **112**, E4306-4315 (2015).
12. Wu, J.-J. *et al.* Inhibition of cGAS DNA Sensing by a Herpesvirus Virion Protein. *Cell Host Microbe* **18**, 333–344 (2015).

13. Kerur, N. *et al.* IFI16 acts as a nuclear pathogen sensor to induce the inflammasome in response to Kaposi Sarcoma-associated herpesvirus infection. *Cell Host Microbe* **9**, 363–375 (2011).
14. Kato, K., Omura, H., Ishitani, R. & Nureki, O. Cyclic GMP-AMP as an Endogenous Second Messenger in Innate Immune Signaling by Cytosolic DNA. *Annu Rev Biochem* **86**, 541–566 (2017).
15. Satija, R., Farrell, J. A., Gennert, D., Schier, A. F. & Regev, A. Spatial reconstruction of single-cell gene expression data. *Nature Biotechnology* **33**, 495–502 (2015).
16. Butler, A., Hoffman, P., Smibert, P., Papalexi, E. & Satija, R. Integrating single-cell transcriptomic data across different conditions, technologies, and species. *Nature Biotechnology* **36**, 411–420 (2018).
17. Arias, C. *et al.* KSHV 2.0: a comprehensive annotation of the Kaposi's sarcoma-associated herpesvirus genome using next-generation sequencing reveals novel genomic and functional features. *PLoS Pathog.* **10**, e1003847 (2014).
18. Majerciak, V. *et al.* A Viral Genome Landscape of RNA Polyadenylation from KSHV Latent to Lytic Infection. *PLOS Pathogens* **9**, e1003749 (2013).
19. Jenner, R. G., Albà, M. M., Boshoff, C. & Kellam, P. Kaposi's Sarcoma-Associated Herpesvirus Latent and Lytic Gene Expression as Revealed by DNA Arrays. *J. Virol.* **75**, 891–902 (2001).
20. Lu, M. *et al.* Dissection of the Kaposi's Sarcoma-Associated Herpesvirus Gene Expression Program by Using the Viral DNA Replication Inhibitor Cidofovir. *J. Virol.* **78**, 13637–13652 (2004).

21. Gabaev, I., Williamson, J. C., Crozier, T. W. M., Schulz, T. F. & Lehner, P. J. Quantitative Proteomics Analysis of Lytic KSHV Infection in Human Endothelial Cells Reveals Targets of Viral Immune Modulation. *Cell Reports* **33**, 108249 (2020).
22. Zhao, M., Zhang, J., Phatnani, H., Scheu, S. & Maniatis, T. Stochastic Expression of the Interferon-β Gene. *PLOS Biology* **10**, e1001249 (2012).
23. Yuan, J. *et al.* Identification and Characterization of RHEBL1, a Novel Member of Ras Family, which Activates Transcriptional Activities of NF-Kappa B. *Mol Biol Rep* **32**, 205–214 (2005).
24. Eaglesham, J. B. & Kranzusch, P. J. Conserved strategies for pathogen evasion of cGAS-STING immunity. *Curr Opin Immunol* **66**, 27–34 (2020).
25. Bhowmik, D. & Zhu, F. Evasion of Intracellular DNA Sensing by Human Herpesviruses. *Front. Cell. Infect. Microbiol.* **11**, (2021).
26. Hertzog, J. & Rehwinkel, J. Regulation and inhibition of the DNA sensor cGAS. *EMBO reports* **21**, e51345 (2020).
27. Hopfner, K.-P. & Hornung, V. Molecular mechanisms and cellular functions of cGAS–STING signalling. *Nature Reviews Molecular Cell Biology* **21**, 501–521 (2020).
28. Patil, S. *et al.* Single-cell analysis shows that paracrine signaling by first responder cells shapes the interferon-β response to viral infection. *Sci. Signal.* **8**, ra16–ra16 (2015).
29. Rand, U. *et al.* Multi-layered stochasticity and paracrine signal propagation shape the type-I interferon response. *Molecular Systems Biology* **8**, 584 (2012).
30. Fiege, J. K. *et al.* Single cell resolution of SARS-CoV-2 tropism, antiviral responses, and susceptibility to therapies in primary human airway epithelium. *PLOS Pathogens* **17**, e1009292 (2021).

31. Sun, J. *et al.* Single cell heterogeneity in influenza A virus gene expression shapes the innate antiviral response to infection. *PLOS Pathogens* **16**, e1008671 (2020).

32. Kallfass, C., Lienenklaus, S., Weiss, S. & Staeheli, P. Visualizing the Beta Interferon Response in Mice during Infection with Influenza A Viruses Expressing or Lacking Nonstructural Protein 1. *Journal of Virology* **87**, 6925–6930 (2013).

33. Wimmers, F. *et al.* Single-cell analysis reveals that stochasticity and paracrine signaling control interferon-alpha production by plasmacytoid dendritic cells. *Nature Communications* **9**, 3317 (2018).

34. Stürzl, M., Gaus, D., Dirks, W. G., Ganem, D. & Jochmann, R. Kaposi's sarcoma-derived cell line SLK is not of endothelial origin, but is a contaminant from a known renal carcinoma cell line. *International Journal of Cancer* **132**, 1954–1958 (2013).

35. Sancak, Y. *et al.* The Rag GTPases Bind Raptor and Mediate Amino Acid Signaling to mTORC1. *Science* **320**, 1496–1501 (2008).

36. Dull, T. *et al.* A Third-Generation Lentivirus Vector with a Conditional Packaging System. *Journal of Virology* **72**, 8463–8471 (1998).

37. Tirosh, I. *et al.* Dissecting the multicellular ecosystem of metastatic melanoma by single-cell RNA-seq. *Science* **352**, 189–196 (2016).

Figure legends

Figure 1. Caspase activity prevents cGAS activation during KSHV lytic replication to block IFN-β induction

(A-E) iSLK.219 cells were transfected with a negative control siRNA, or siRNAs targeting STING (A,B), MAVS (A,B), cGAS (C-E), or IFI16 (C,D). For cGAS, the transfection was carried out twice, two days prior to and on the day of lytic cycle induction; for STING, MAVS and IFI16, one transfection was carried out two days prior to induction. The cells were then lytically reactivated with doxycycline (1 μg/ml) and treated with either DMSO (vehicle), IDN-6556 (10 μM) and/or the cGAS inhibitor RU.521 (cGASi, 24.1 μM) as indicated. (A-D) Total RNA was extracted at day 5 post reactivation and the levels of IFN-β (A,C) and ORF37 (B,D) mRNA were measured by RT-qPCR and normalized to levels of 18S rRNA ($n \geq 3$). (E) Cell lysates were harvested at day 4 post reactivation and subjected to western blot for cGAS and β-tubulin as a loading control. Blots are representative of 3 repeats. (F) Total RNA was extracted from iSLK.219 cells 3 days after reactivation. Levels of IFN-β mRNA were measured by RT-qPCR and normalized to 18S rRNA ($n = 3$). (G) Levels of 2'3'-cGAMP in lysate collected from iSLK.219 cells at day 4 post reactivation were measured by ELISA ($n = 4$). (H) Cell lysates were harvested at day 4 post reactivation and subjected to western blot for p-TBK-1, TBK-1, p-IRF-3, IRF-3, p-STING, STING, and β-tubulin (as a loading control) as indicated. Blots are representative of 3 repeats.

ns, *, **, ***, ****: *p* value > 0.05, < 0.05, < 0.01, < 0.001, < 0.0001, Tukey's multiple comparisons test (Dox+vehicle vs. Dox+IDN-6556, or indicated comparison) after two-way ANOVA.

Figure 2. Caspases also inhibit cGAS activity in KSHV infected B cells

BC3 cells were lytically reactivated with TPA (20 ng/ml) for 1-3 days as indicated (A) or for 2 days (B-G) and treated with DMSO (vehicle), the pan-caspase inhibitor IDN-6556 (10 μM), or the cGAS inhibitor RU.521 (cGASi, 24.1 μM) as indicated. (A) Cell lysates were collected from lytically reactivated BC3 cells at the indicated time points and subjected to western blot analysis for activated (cleaved) caspase-8, and β-tubulin as a loading control. Blots are representative of 3 repeats. (B-D) Total RNA was extracted from BC3 cells. Levels of IFN-β (B), ISG15 (C), IFIT1 (D) mRNA were measured by RT-qPCR and normalized to 18S rRNA (n = 3). (E) Levels of 2'3'-cGAMP in lysate collected from BC3 were measured by ELISA (n = 4). (F) Cell lysates were collected from lytically reactivated BC3 cells and subjected to western blot analysis for activated p-IRF3, total IRF3, and β-actin as a loading control. Blots are representative of 3 repeats. (G) Total RNA was extracted from BC3 cells. Levels of IFN-β mRNA were measured by RT-qPCR and normalized to 18S rRNA (n = 3). *, ****: *p* value < 0.05, < 0.0001, Tukey's multiple comparisons test after two-way ANOVA.

Figure 3. Single-cell RNAseq analysis reveals subsets of lytically reactivating cells. (A) Diagram of the single-cell RNAseq (scRNAseq) experiment using 4 samples. Sample 1 was a mixture of uninfected iSLK.RTA and latently infected iSLK.219 cells treated with DMSO

(vehicle). Samples 2-4 were iSLK.219 treated with doxycycline (Dox) to reactivate lytic replication ("Lytic") and treated with DMSO (vehicle), the caspase inhibitor IDN-6556, or the caspase inhibitor IDN-6556 and a cocktail of anti-IFN antibodies to block paracrine IFN signaling. All samples were collected 4 days after the start of treatments. (B-G) Analysis of data from the scRNAseq experiment presented in (A). (B) UMAP diagram of the clusters unbiasedly defined by Seurat in the 4 samples. (C) UMAP diagram showing what percentage of reads from each cell comes from the KSHV genome. Legends on the right define what percentage the colors represent. (D) Violin plot of the distribution of cells in each sample based on percentage of KSHV reads. Sample 1 has a bimodal distribution because it is a mix of uninfected and latent cells. (E) Heatmap of expression of individual KSHV genes in each cell in the lytic + vehicle sample, sorted by cluster. Cluster labeling ("uninfected", "latent" etc.) was based on this analysis, as well as analysis of the cell cycle stage of the cells (Supp. Fig. 3G). (F-G) Plot of percentage reads per cell that map to each of three types of KSHV genes (latent, early and late) in each cluster in the lytic + vehicle sample. Clusters are sorted based on the total average % of KSHV reads. (H) Pie-charts of percentage of cells that map to each cluster in the four samples.

Figure 4. Only a small fraction of KSHV lytic cells express IFN-β. (A-G) Analysis of data from the scRNAseq experiment presented in Fig. 3A. (A) UMAP diagram of the clusters unbiasedly defined by Seurat in the 3 lytic samples (same as Fig. 3B). (B-C) UMAP diagram of the level of expression of IFN-β (B) or ISG15 (C) in each cell. The legends on the right define what expression level the colors represent (arbitrary units). (D-G) Heat maps of expression of specific genes in each cell, sorted by clusters, for the lytic+IDN-6556 (D,F) and the lytic+IDN-6556+anti-IFNs samples (E,G). In D,E viral genes are listed for clusters classified as "Lytic

(early)", "Lytic (intermediate)", and "Lytic (early) + IFN". In F,G select genes from the type I IFN induction pathway are listed for all clusters. The legends on the right define what expression level the colors represent (arbitrary units). (H) iSLK.219 were treated with doxycycline to reactivate the lytic cycle ("lytic") and IDN-6556, where indicated. Protein lysates were collected at day 4 and analyzed by western blotting for NF-κB, phospho-NF-κB and β-tubulin as a loading control. (I) iSLK.219 expressing TagBFP from a human IFN-β promoter were treated with doxycycline to reactivate the lytic cycle ("lytic") and IDN-6556, where indicated. Flow cytometry was carried out on the cells 4 days after doxycycline addition. RFP axis reflects the RFP signal in lytic cells and BFP axis reflects activity of the IFN-β promoter. Percentage of cells mapping to each quadrant are listed. Flow cytometry plots are representative of 3 repeats.

Supplemental Figure legends

Figure S1. Knockdown of proteins in the type I IFN induction pathway.

iSLK.219 cells were transfected with a negative control siRNA and siRNAs targeting STING, MAVS, cGAS, or IFI16. (A, C) Cell lysates were harvested at day 4 post reactivation with doxycycline and subjected to western blot for the target proteins and β-actin or β-tubulin as loading controls. Blots are representative of 3 repeats. (B,D) iSLK.219 cells were transfected with either plasmid DNA (400 ng/ml; B,D) or poly(I:C)-Lyovec (5 μg/ml; B). Total RNA was extracted 3 hours post transfection and the levels of IFN-β mRNA were measured by RT-qPCR ($n \geq 3$). ns, *, **, ***, ****: p value > 0.05, < 0.05, < 0.01, < 0.001, < 0.0001, Tukey's multiple comparisons test (Dox+vehicle vs. Dox+IDN-6556, or indicated comparison) after two-way ANOVA.

Figure S2. cGAS inhibition counteracts the effects of caspase inhibition on IFN signaling in KSHV-infected cells.

iSLK.219 were lytically reactivated with doxycycline (1 μg/ml) for 3 days and BC3 cells were lytically reactivated with TPA (20 ng/ml) for 2 days. Cells were treated with DMSO (vehicle), IDN-6556 (10 μM), or the cGAS inhibitor RU.521 (cGASi, 24.1 μM) as indicated. Levels of ISG15 and IFIT1 mRNA were measured by RT-qPCR and normalized to 18S rRNA (n = 3). ns, *, **, ***: *p* value > 0.05, < 0.05, < 0.01, < 0.001, Tukey's multiple comparisons test (Dox+vehicle vs. Dox+IDN-6556, or indicated comparison) after two-way ANOVA.

Figure S3. scRNAseq controls and results. (A-D) iSLK.219 cells were treated with doxycycline (1 μg/ml) to reactivate the lytic cycle, as well as IDN-6556 and anti-IFN antibodies where indicated. mRNAs levels of IFN- β (A), the ISGs ISG15 and IFIT1 (B-C), and the KSHV gene ORF37 (D) were measured by RT-qPCR four days after doxycycline addition. (E-G) Analysis of data from the scRNAseq experiment presented in Figure 3A. (E-F) (E) Heatmaps of expression of individual KSHV genes in each cell in the lytic + IDN-6556 and lytic +IDN-6556 + anti-IFN samples, sorted by cluster. Cluster labeling ("uninfected", "latent" etc.) was based on analysis in Fig. 3, as well as analysis of the cell cycle stage of the cells in panel G. (G) UMAP diagram of cell cycle stage classification of cells in the 4 samples.

Figure 1

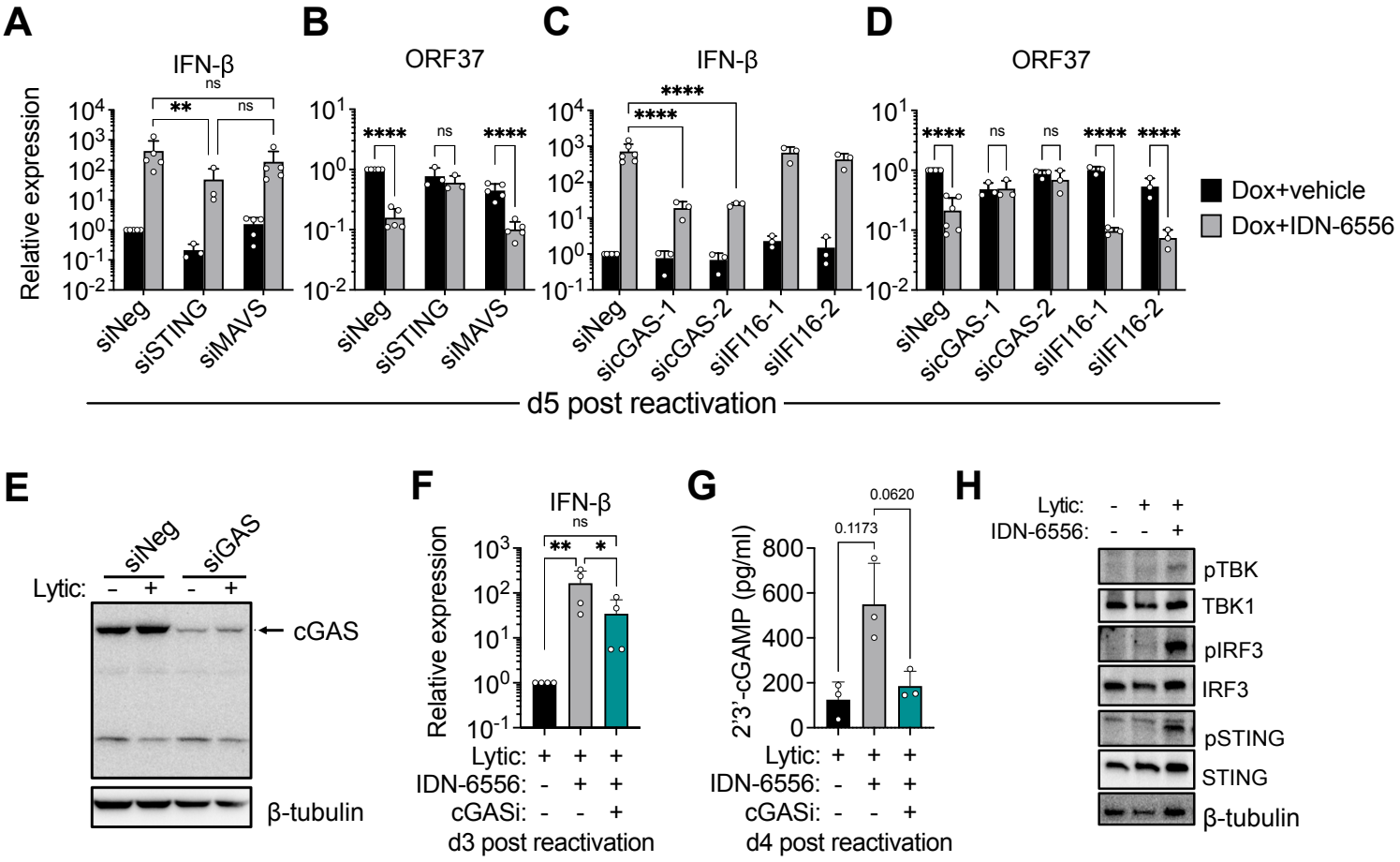
A
IFN-β
Relative expression
siNeg
siSTING
siMAVS
B
ORF37
C
IFN-β
siNeg
sicGAS-1
sicGAS-2
siIFI16-1
siIFI16-2
D
ORF37
Dox+vehicle
Dox+IDN-6556
d5 post reactivation
E
siNeg
siGAS
Lytic:
cGAS
β-tubulin
F
IFN-β
Relative expression
Lytic:
IDN-6556:
cGASi:
d3 post reactivation
G
2'3'-cGAMP (pg/ml)
0.1173
0.0620
d4 post reactivation
H
Lytic:
IDN-6556:
pTBK
TBK1
pIRF3
IRF3
pSTING
STING
β-tubulin

Figure 2

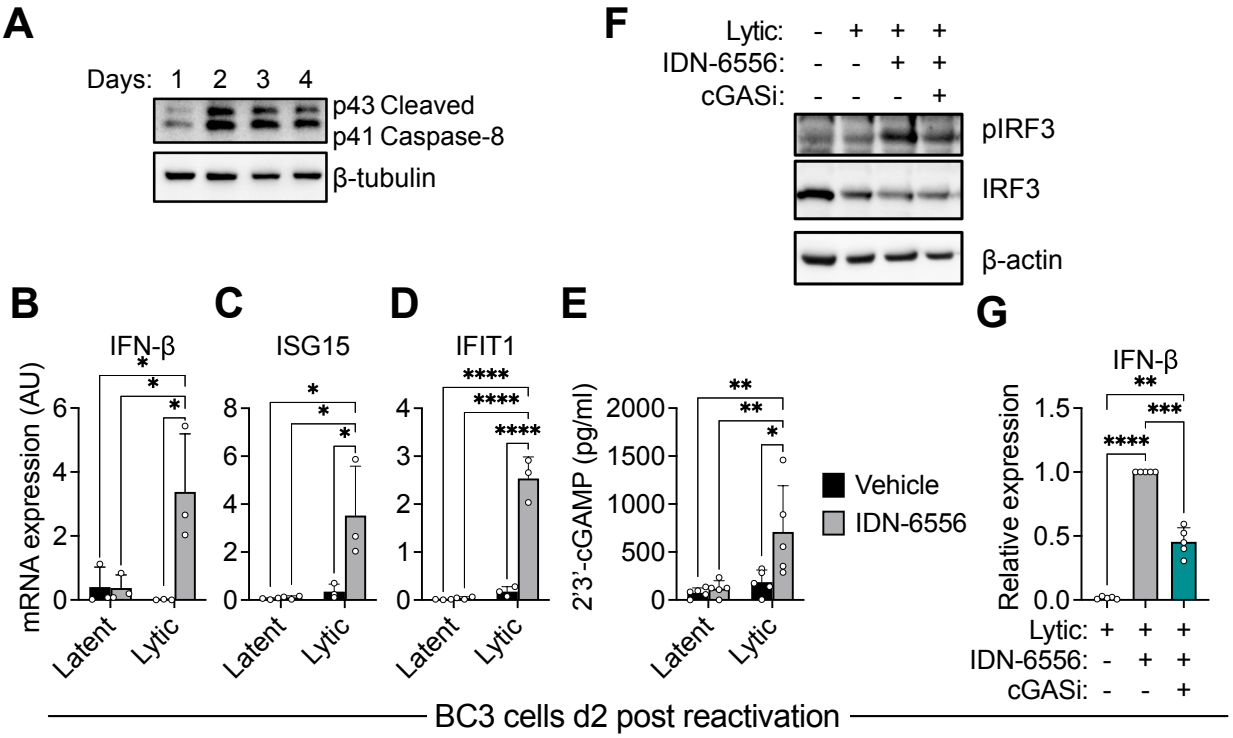
A
Days: 1 2 3 4
p43 Cleaved
p41 Caspase-8
β-tubulin
F
Lytic: - + + +
IDN-6556: - - + +
cGASi: - - - +
pIRF3
IRF3
β-actin
B
IFN-β
mRNA expression (AU)
Latent
Lytic
C
ISG15
D
IFIT1
E
2'3'-cGAMP (pg/ml)
Vehicle
IDN-6556
G
IFN-β
Relative expression
Lytic: + + +
IDN-6556: - + +
cGASi: - - +
BC3 cells d2 post reactivation

Figure 3

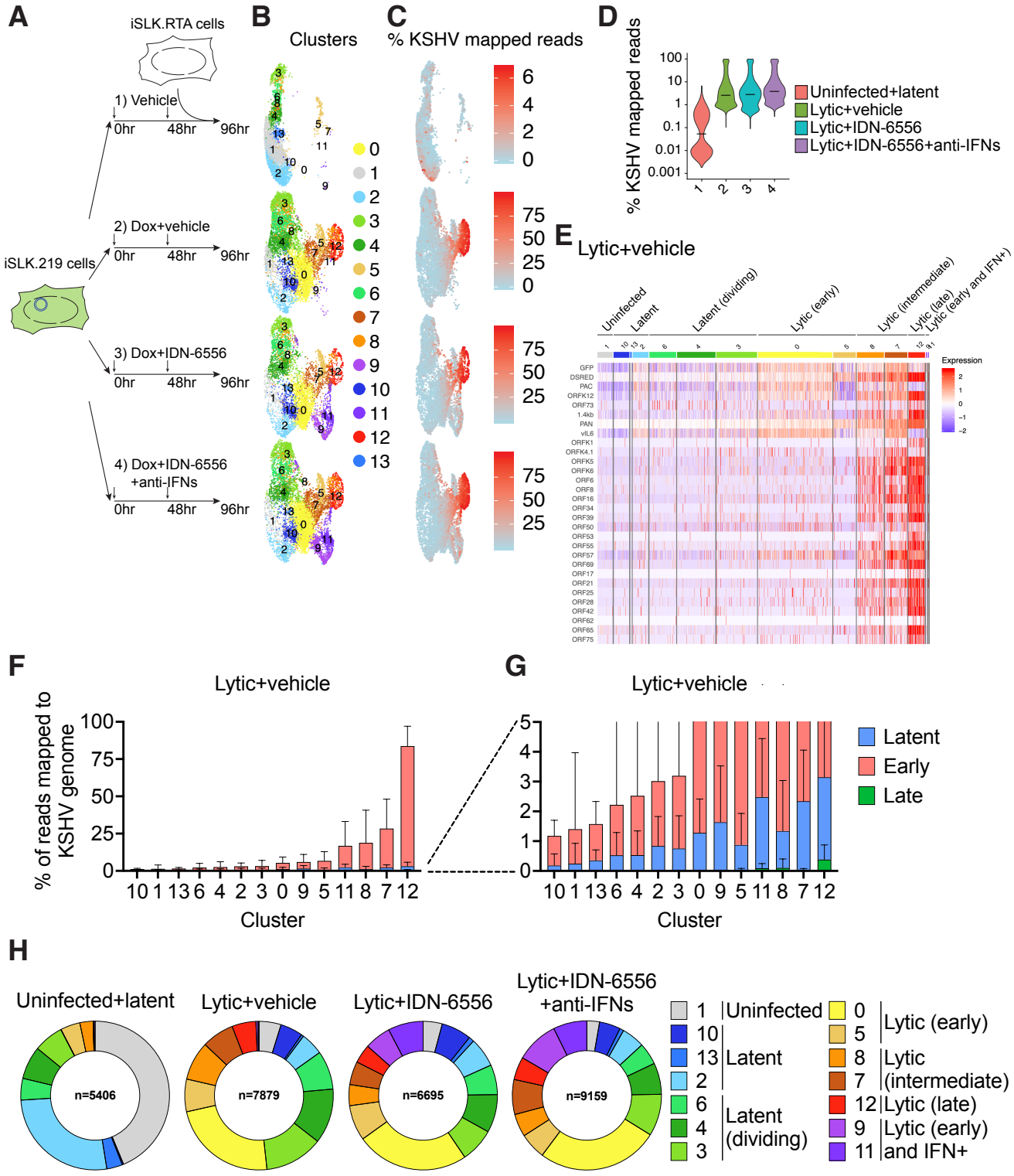
A
iSLK.RTA cells
1) Vehicle
0hr
48hr
96hr
iSLK.219 cells
2) Dox+vehicle
3) Dox+IDN-6556
4) Dox+IDN-6556
+anti-IFNs
B
Clusters
C
% KSHV mapped reads
D
% KSHV mapped reads
Uninfected+latent
Lytic+vehicle
Lytic+IDN-6556
Lytic+IDN-6556+anti-IFNs
E
Lytic+vehicle
Uninfected
Latent
Latent (dividing)
Lytic (early)
Lytic (intermediate)
Lytic (late)
Lytic (early and IFN+)
Expression
F
Lytic+vehicle
% of reads mapped to KSHV genome
Cluster
G
Lytic+vehicle
Latent
Early
Late
Cluster
H
Uninfected+latent
Lytic+vehicle
Lytic+IDN-6556
Lytic+IDN-6556
+anti-IFNs
n=5406
n=7879
n=6695
n=9159
Uninfected
Latent
Latent
(dividing)
Lytic (early)
Lytic
(intermediate)
Lytic (late)
Lytic (early)
and IFN+

Figure 4

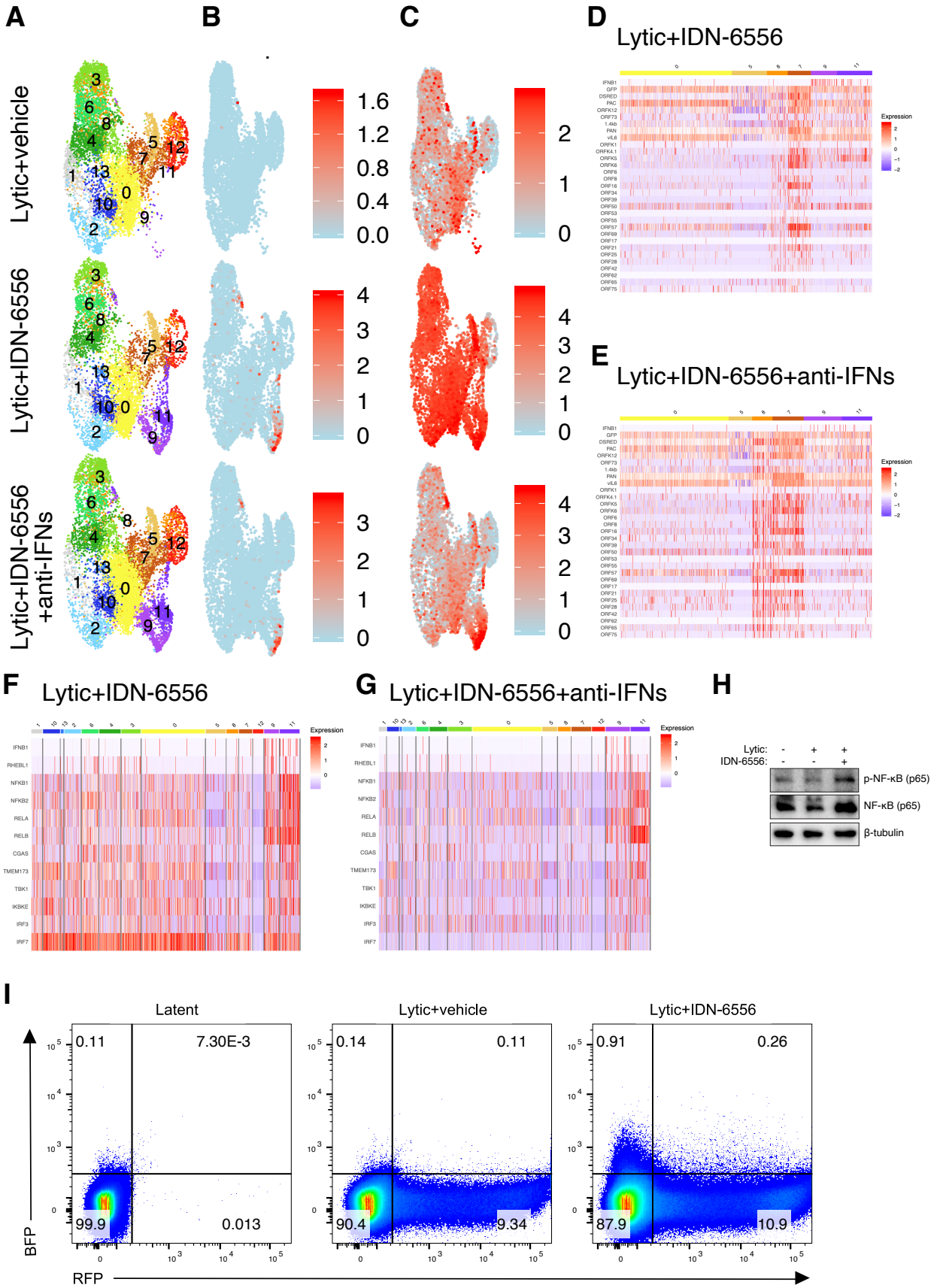
A
B
C
D
Lytic+IDN-6556
E
Lytic+IDN-6556+anti-IFNs
Lytic+vehicle
Lytic+IDN-6556
Lytic+IDN-6556 +anti-IFNs
F
Lytic+IDN-6556
G
Lytic+IDN-6556+anti-IFNs
H
Lytic:
IDN-6556:
p-NF-κB (p65)
NF-κB (p65)
β-tubulin
I
Latent
Lytic+vehicle
Lytic+IDN-6556
0.11
7.30E-3
99.9
0.013
0.14
0.11
90.4
9.34
0.91
0.26
87.9
10.9
BFP
RFP